ÉCOLE POLYTECHNIQUE
FÉDÉRALE DE LAUSANNE

LPHE

Detection of K(892)^{0*} from first data at LHCb

Master TP IV

July 12, 2010

Léonie Berge
leonie.berge@epfl.ch

Contents

1 Introduction

The Large Hadron Collider (LHC), at CERN in Geneva, is a circular particle accelerator which sends two opposite beams of protons in order to get head-on collisions at very high energy. On March 30th the total energy reached 7 TeV in the center of mass, i.e. 3.5 TeV for each proton beam.
These collisons provide data for several experiments. The data are collected by four detectors : ATLAS, CMS, ALICE and LHCb. The "mission" of the LHCb detector is to study B-physics (quark b), which gives precious information about CP-violation. It is composed of several types of detectors (see Figure 1) : trackers and dipole magnet to measure the momentum of charged particles, electromagnetic and hadronic calorimeters, Cherenkov detectors and muon chambers, which allow complete and accurate reconstruction of each detected event [1].
The goal of this work is to study the $K(892)^{0*}$, through the decay $K\,(892)^{0*} \longrightarrow K^{+}\pi^{-}$, with data taken at LHCb in April 2010.

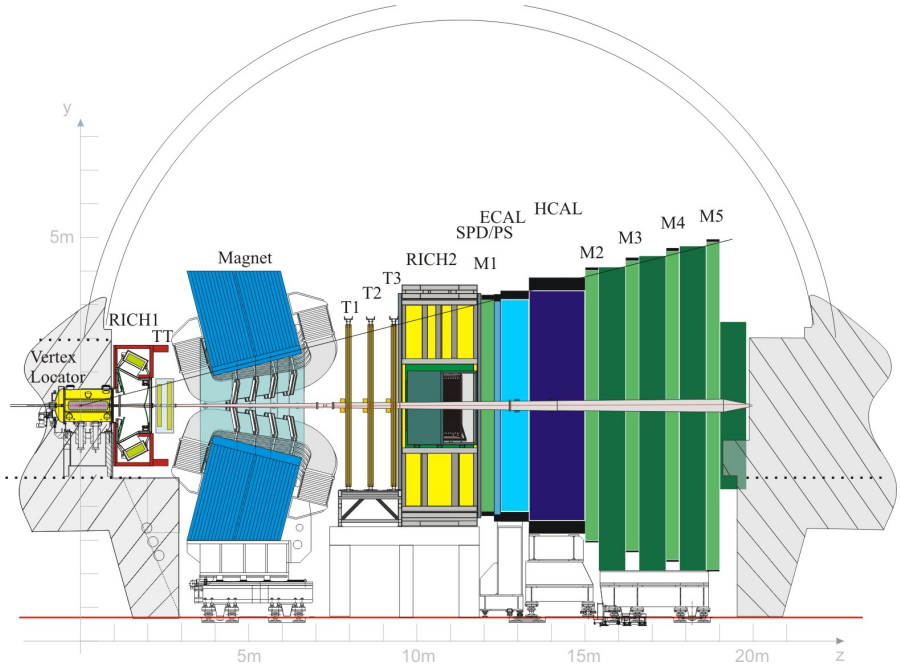

Figure 1: LHCb detector

2 K^{0*} production

Various mechanisms can lead to a K^{0*} production in LHCb :

- it can be produced directly in the primary vertex (PV), i.e. the hadrons collision point : these K^{0*} are called "prompt" K^{0*} ;
- it can come from a B decay ;
- it can also come from a D decay.

We have proceeded with three steps. We started with Monte-Carlo simulation data, in which we have everything that comes from a prompt B^0. Then we tried to see if we still had some results with minimum bias simulation data, and finally we looked at the real data.

The B^0 $(d\bar{b})$ major decay modes are [2] :

1. Semi-leptonic decays : $B^0 \longrightarrow l + \nu_l + anything$
2. Hadronic decays :
   - $b \to c$ transitions (most frequent)
   - $b \to u$ and $b \to s$ transitions (suppressed)

The decay mode we will focus on for the initial Monte-Carlo data :

$$B^0 \longrightarrow K(892)^{0*} + \eta^0 \tag{1}$$

happens with a $(1.59 \pm 0.10) \cdot 10^{-5}$ probability [2].

The daughter particles will then decay in

$$\begin{cases} K^{0*} & \longrightarrow & K^+ & + & \pi^- & 66\% \\ \eta & \longrightarrow & \gamma & + & \gamma & (39.30 \pm 0.20)\% \end{cases}$$

The main characteristics of $K(892)^{0*}$ are listed in Table 1.
Because the K^* decays through strong interaction, it has a very short lifetime, and therefore a very large decay width and very short flight distance. Let's estimate its flight distance in the lab frame ($\beta \sim 1 \Rightarrow E \sim p$) :

$$d_{flight} = v \cdot t = (\beta c)\,(\gamma\tau) \tag{2}$$

Mass M	[MeV/c^2]	896.00 ± 0.25
Full width Γ	[MeV]	50.3 ± 0.6
Lifetime $\tau = \hbar/\Gamma$	[s]	$1.23 \cdot 10^{-23}$

Table 1: $K(892)^{0*}$ parameters [2]

with

$$\beta\gamma \approx \frac{p}{M} \sim 10 \tag{3}$$

where we assumed $p \sim 10$ GeV.

We find

$$d_{flight} \sim 50 \text{ fm} \tag{4}$$

which is negligible in regard to the resolution of the detector, which is around 10 μm ; we can thus consider that the K^+ and π^- come from the K^{0*} production vertex. The η leaves no track since it is neutral, and we can reconstruct it by the two photons we see in the calorimeter.

The Figure 2 shows a schematic view of the topology of this decay.

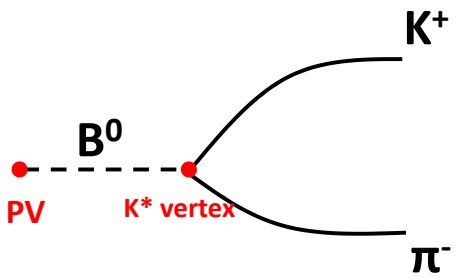

Figure 2: B^0 decay

3 K^{0*} candidates reconstruction

The main tool for this study has been the CERN program named ROOT [3]. We used a code called HFAna, which is based on the DaVinci framework. Through all the data, HFAna selects the potential K^{0*} according to some selection criteria, and stores them in a Ntuple, i.e. a tabular on ROOT format. With the help of ROOT we can edit histograms and fits. We wrote a macro to add some selections we wanted to apply, and created a new ROOT file with the candidates that passed the new selection. It it then easier to work on this new file (Figure 3).

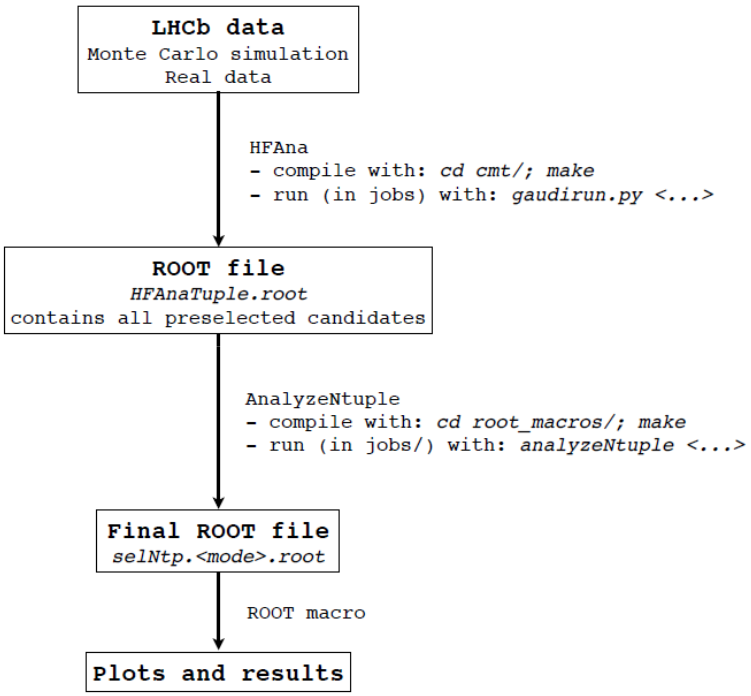

Figure 3

It is good to introduce some of the important variables of HFAna Ntuple as a first step. To subtract enough background, we will impose conditions on these variables.

Transverse momenta

The transverse momentum of one particle is its transverse momentum with respect to the axis of the beams (Figure 4).

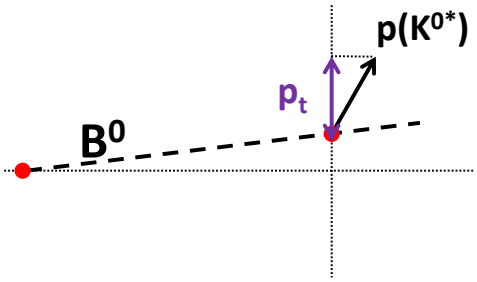

Figure 4: Transverse momentum of K^* (the horizontal dotted line represents the axis of the protons)

In the case of our first simulation data, all the candidates are coming from B^0 following the decay described in equation 1 :

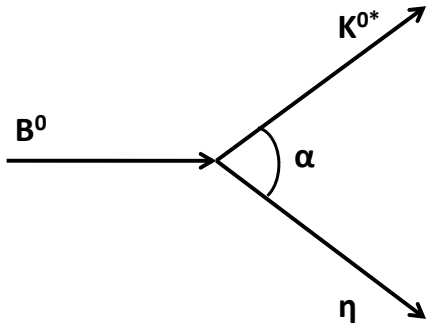

The conservation of the energy-momentum gives :

$$M_B^2 = M_K^2 + M_\eta^2 + 2E_K E_\eta - 2p_K \cdot p_\eta \cdot \cos\alpha \tag{5}$$

Since the B^0 is more massive than its daughter particles, they are emitted with a large α with respect to the B^0 propagation axis (assuming $p_K \sim p_\eta \sim$ 10 GeV, and knowing $M_\eta = 548 MeV/c^2$ and $M_B = 5280 MeV/c^2$, we find $\alpha \sim 30°$). We can assume that this axis is not so different from the proton beams axis ; thus in average we must have high values of p_t for the K^* from B decays.

Flight distance

We have seen that the K^* decays instantaneously ; due to a particularity of the program, the HFAna "Kst_flightDist" variable, that we will write $d(PV, K^*)$, actually refers to the distance between the primary vertex and the K^0 vertex (which is close to the flight distance of the B^0).

PVDOCA

The primary vertex distance of closest approach (PVDOCA) of the K^*, $PVDOCA(K^*)$, is the shortest distance between the PV and the momentum direction of the K^* (Figure 5).
We will also consider the $\chi^2\,(PVDOCA)_{K^+}$ (resp. $\chi^2\,(PVDOCA)_{\pi^-}$), as the χ^2 of the $PVDOCA(K^+)$ (resp. of the $PVDOCA(\pi^-)$), which has to be as large as possible[1].

[1]Reminder : the χ^2 is defined by

$$\chi^2(x) = \sum_{i=0} \frac{(x_i - \overline{x})^2}{\sigma_i^2}$$

where :
x is a random variable
$\overline{x}$ is the average of the variable x
σ_i is the uncertainty about the measurement of x_i.

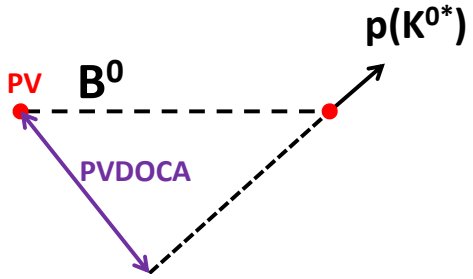

Figure 5: K^{0*} PVDOCA

χ^2 of the vertex of the K^{0*}

We reconstruct a particle (K^+ or π^-) from the track it leaves in the tracker. We define the quality of the K^* decay vertex, by the χ^2 of the vertex fit for the $K^+\pi^-$, that we will call χ^2 (K^*vertex).

Another interesting variable is the $DOCA\,(track, vertex)$: it is the DOCA between the $K^+\pi^-$ reconstructed vertex and the nearest track seen around this vertex. If it is too short there is a non-negligible probability that this nearest track also comes from the vertex, then it would no longer be a good K^{0*} vertex candidate.

Particle identification : Difference of Log-Likelihood (DLL)

The particle identification is made by looking at the characteristics of one track, but we always have a probability to be mistaken about the particle identity. The DLL is an indicator of the probability for a detected particle to be a given particle (rather than a pion, so the DLL_π is always zero) :
$DLL_K(K^+)$ is the likelihood that our K^+ is an actual kaon, and not a fake one. It has to be as high as possible.
$DLL_p(\pi^-)$ is the likelihood that our π^- is a proton, we want it to be as small as possible.
$DLL_K(\pi^-)$ is the likelihood that our π^- is a kaon, we want it to be as small as possible.

4 "Preselected" Monte-Carlo

As explained above, we began the study on Monte-Carlo simulation data with everything that comes from a B^0. We have a total number of events of 9800. Figure 6 shows the histogram of the reconstructed mass of the K^*, without additional cuts.

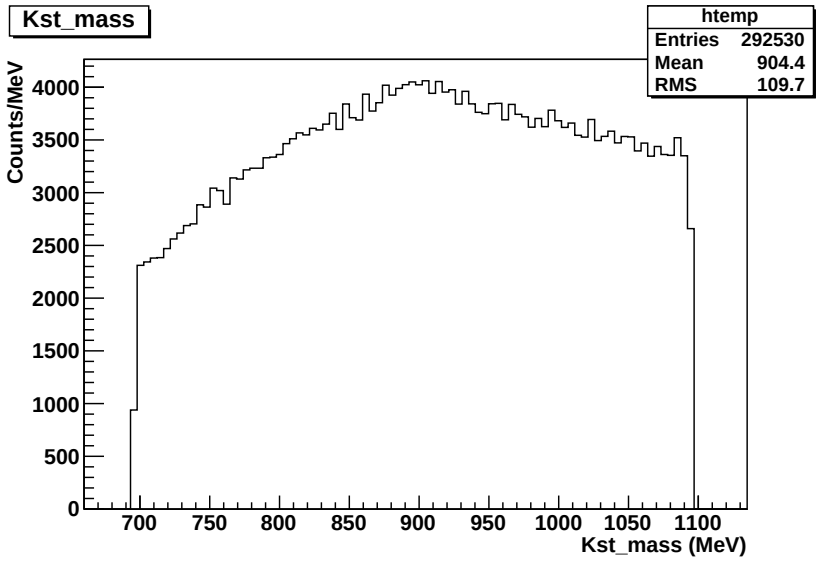

Figure 6: Reconstructed mass of the K* without additional cuts

Since this is simulation data, we can actually know which candidates are real K^{0*}, coming directly from B^0. This is very useful, and we can look at the distribution for the different variables of the "real K^{0*}" and compare it with the distributions of all the K^* (prompt and secondary), so we can see where to apply the cuts. If we look at the distribution of the K^* transverse momentum for the true K^* (Figure 7a), a peak is clearly visible around 2-3 GeV. Thus, demanding a p_{t,K^*} above 2 GeV seems not to reject too much signal. Applying this condition therefore contributes to reducing the background. In our case we see that it really helps (Figure 7b), most of our reconstructed K^* being below 2 GeV of p_t.

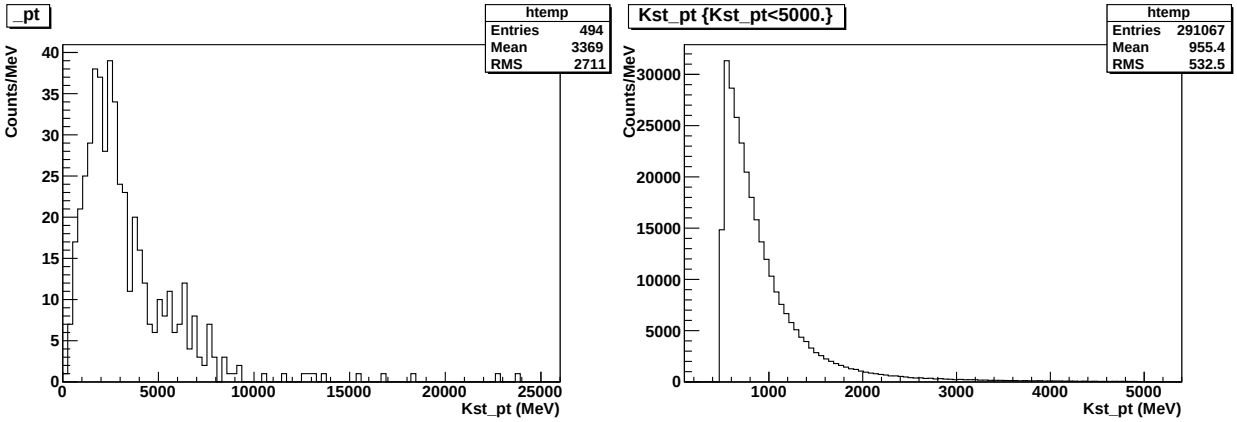

(a) (b)

Figure 7: Distribution of p_{t,K^*} for : (a) Monte-Carlo data with only true K^* coming from B^0 (b) all Monte-Carlo reconstructed candidates.
No events before 500 MeV, because of a primary cut applied at $p_{t,K^*} > 500$ MeV at DaVinci level.

After examining all the variables, the final cuts applied were :

$p_t(K*)$	$>$	2 GeV
$d(PV, K^*)$	$<$	100 mm
$\chi^2\,(K^*\text{vertex})$	$<$	10.0
$\chi^2\,(PVDOCA)_{K^+,\pi^-}$	$>$	10.0
$DLL_K\,(K^+)$	$>$	5.0

The evolution of the peak throughout the different cuts is presented in Figure 8, and Figure 9 shows the distributions of the variables which we cut.

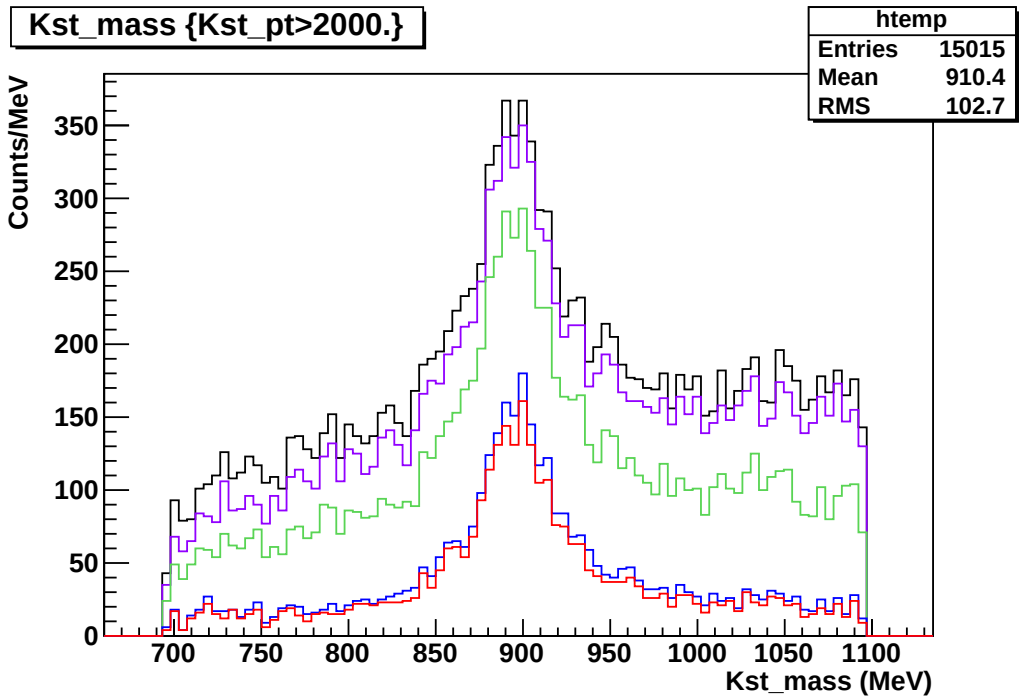

Black	: $p_t(K*) > 2$ GeV	
Purple	: Same cuts as for black histogram	$+\ d(PV, K^*) < 100$ mm
Green	: Same cuts as for purple histogram	$+\ \chi^2\,(K^*\text{vertex}) < 10.0$
Blue	: Same cuts as for green histogram	$+\ \chi^2\,(PVDOCA)_{K^+,\pi^-} > 10.0$
Red	: Same cuts as for blue histogram	$+\ DLL_K\,(K^+) > 5.0$

Figure 8

To fit the signal peak, we had to use a sum of two functions : one for the K^{0*} peak and the second one for the background, which we estimated linear in this case.
In a first approach, we fitted the signal with a gaussian :

$$G\,(E) = N_s \left(\frac{l_{bin}}{\sigma\sqrt{2\pi}} \right) e^{-\frac{1}{2}\left(\frac{E-M}{\sigma}\right)^2} \tag{6}$$

and the background by a linear function :

$$b\left(E\right) = \frac{N_b}{N_{bin}}\left[1 + a_b\left(E - E_0\right)\right] \tag{7}$$

with E_0 the center of the energy range, l_{bin} the width of one bin in MeV and N_{bin} the number of bins.

The fit function was then :

$$total\left(E\right) = G\left(E\right) + b\left(E\right) \tag{8}$$

The program takes five parameters with an initial value and returns the "best fitting" value, so we get :

P_0	$\rightarrow$	N_s	:	Number of signal counts
P_1	$\rightarrow$	M	:	Mass of the K^{0*}
P_2	$\rightarrow$	σ	:	Width of the Gaussian
P_3	$\rightarrow$	N_b	:	Number of background counts
P_4	$\rightarrow$	a_b	:	Background slope

The fit is presented in Figure 10a.

To be more accurate for the representation of the signal shape, we replaced the Gaussian by a Breit-Wigner function [4], of the form :

$$BW\left(E\right) = \frac{1}{N_{norm,BW}} \cdot N_s \cdot l_{bin} \cdot \frac{\Gamma^2}{\left(E - M\right)^2 + \Gamma^2/4} \tag{9}$$

with $N_{norm,BW}$ the normalization factor of the Breit-Wigner for a finite energy interval between E_{min} and E_{max} :

$$N_{norm,BW} = 2\Gamma\left[\arctan\left(\frac{2(E_{max} - M)}{\Gamma}\right) - \arctan\left(\frac{2(E_{min} - M)}{\Gamma}\right)\right] \tag{10}$$

The parameter P_2 is now the width Γ of the K^*. The fit is shown in Figure 10b and its parameters in Table 2. What we called the "efficiency" of the fit, is the number of signal counts over the total number of events before any cuts, and $N_s/\sigma(N_s)$ is the ratio of the number of signal counts over the error on that number. We want this number to be maximum. The $\chi^2 = 1.3$ per

degree of freedom of the fit is close to 1 as we expected for a good fit result (in the following, what we will call the χ^2 of the fit will refer to the χ^2 of the fit per degree of freedom). For the Gaussian fit it is 1.95, so the Breit-Wigner fit is better. This is because the K^* width Γ is larger than the resolution of the detector, so the shape of the peak is dominated by the Breit-Wigner, and not by a Gaussian, like it would have been the case if Γ was much smaller than the resolution Gaussian width.

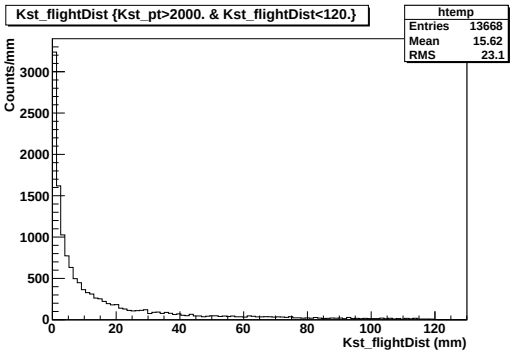

(a) Kst_flightDist with $p_{t,K*} > 2$ GeV

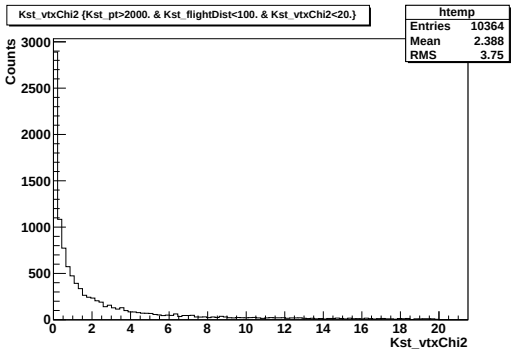

(b) $\chi^2\,(K^*\text{vertex})$, same cuts as (a)+ Kst_flightDist<0.1 m

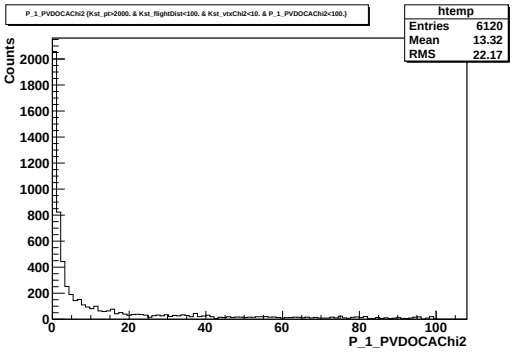

(c) $\chi^2\,(PVDOCA)_{K^+}$, same cuts as (b)+ $\chi^2\,(K^*\text{vertex}) < 10.0$

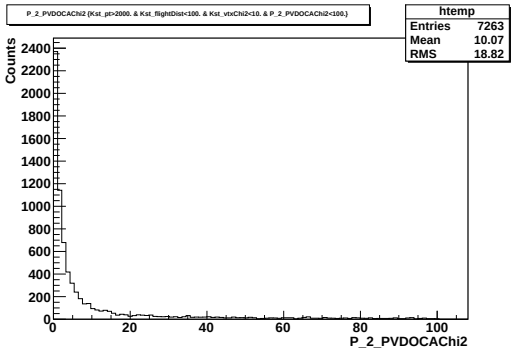

(d) $\chi^2\,(PVDOCA)_{\pi^-}$, same cuts as (c)

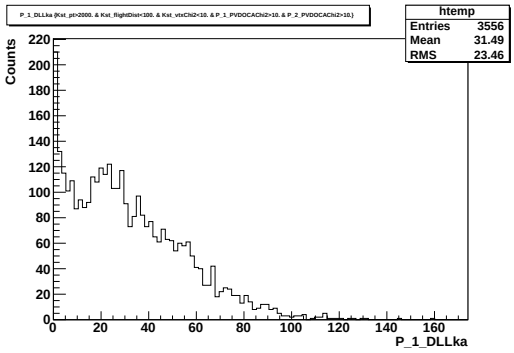

(e) $DLL_K\,(K^+)$, same cuts as (c),(d)+ $\chi^2\,(PVDOCA)_{K^+,\pi^-} > 10.0$

Figure 9: Distribution of the HFAna variables for pre-selected Monte-Carlo (beware of Kst_flightDist which refers to the distance between PV and K* decay vertex)

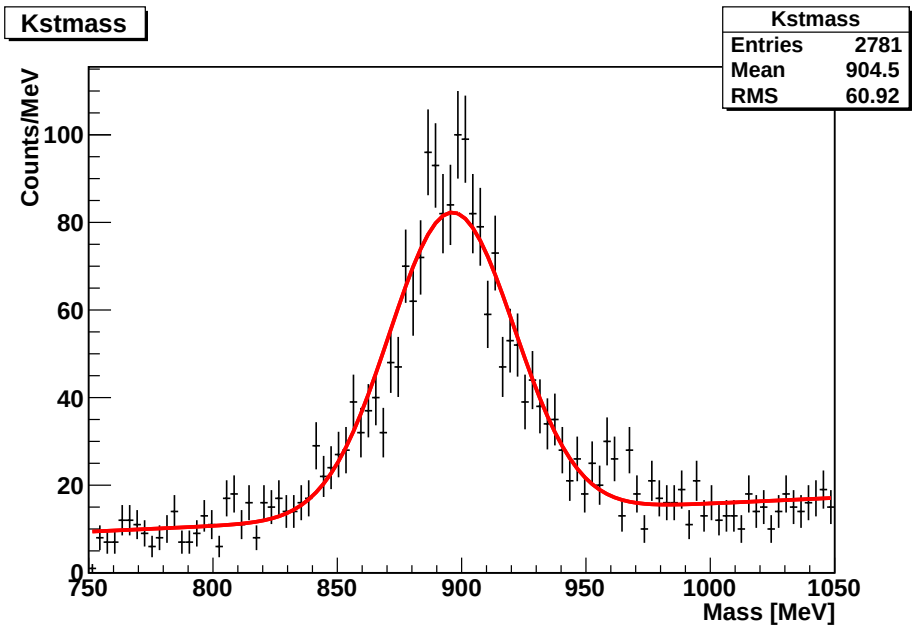

(a) Fit of the reconstructed K^{0*} for the Monte-Carlo preselected data, with a Gaussian function

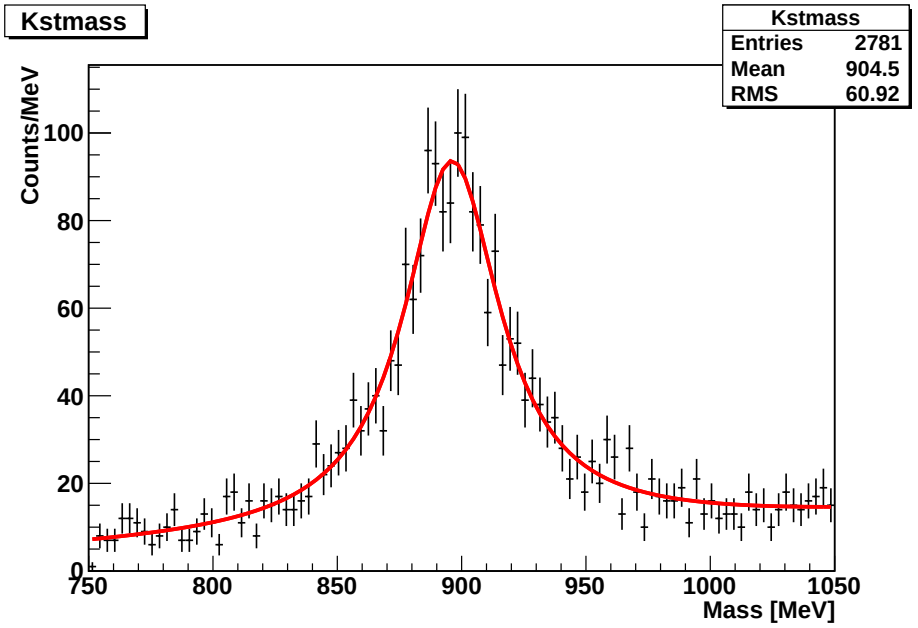

(b) Same fit with a Breit-Wigner

Figure 10

5 Minimum bias simulation

We now have a nice peak, with data coming from B^0. Before dealing with the real data, we must try to get the best possible fit with comparable simulation data, i.e. minimum bias simulation. The data is a MC09 simulation, the energy in the center of mass is 10 TeV, and it contains 3.31 millions of events.

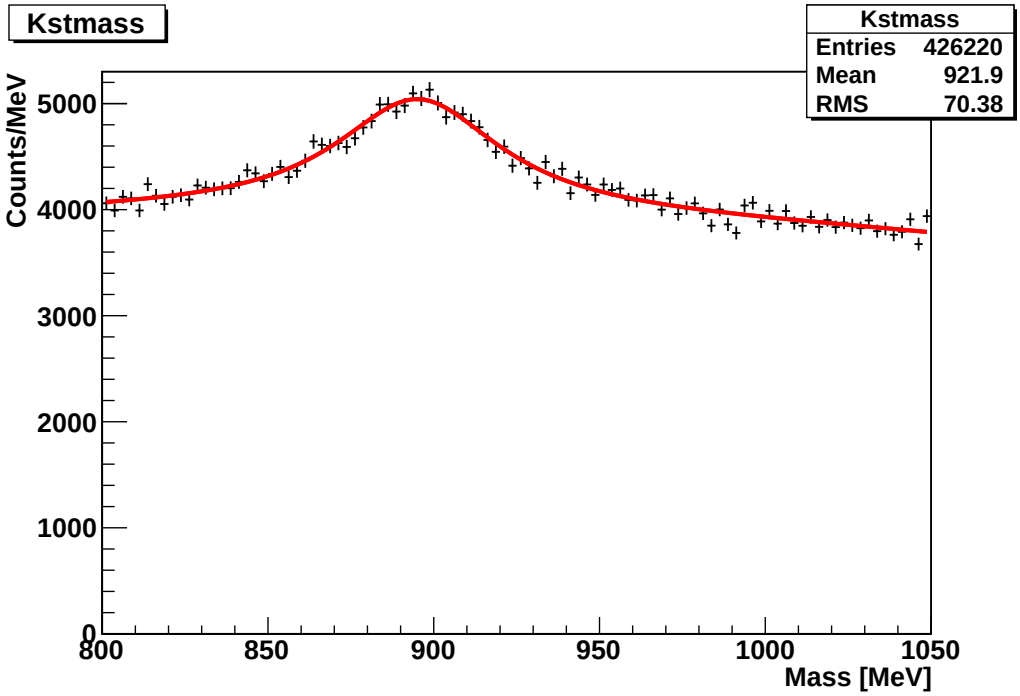

Figure 11: K^{0*} peak, Monte-Carlo, minimum bias

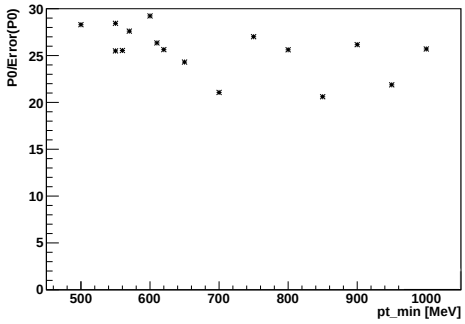

(a) Minimum bias simulation

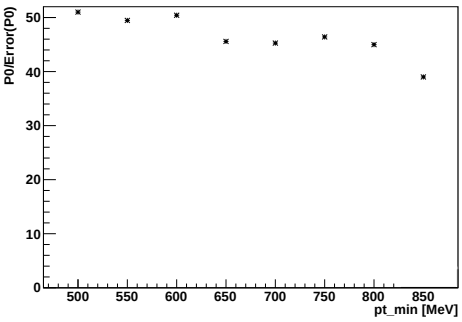

(b) Real data

Figure 12: Ratio of peak signal over error as a function of the cut on transverse momentum (background parameters fixed)

The cuts applied were :

$DLL_K(K^+)$	$>$	25
$DLL_p(\pi^-)$	$<$	-20
$DLL_K(\pi^-)$	$<$	-25
$\chi^2\,(K^*\text{vertex})$	$<$	10.0
$d(PV, K^*)$	$<$	80 mm
$\chi^2\,(PVDOCA)_{K^*}$	$<$	10.0
$DOCA\,(track, vertex)$	$>$	0.02 mm

The cut on $p_t(K^*)$ does not make sense anymore, most of the K^{0*} that we see coming from PV. Figure 12a shows the ratio of signal over error for different cuts on the $p_t(K^*)$ (and for fixed parameters for the background slope and quadratic factor). It does not seem to show any maximum, so we decided to let the cut on the $p_t(K^*)$ at 500 MeV, which was the cut demanded at the DaVinci level and that we could not change ; maybe after all this cut was not even necessary.
The cuts which helped the more on minimum bias Monte-Carlo were the restrictions on $DLL_K(K^+)$, $DLL_p(\pi^-)$ and $DLL_K(\pi^-)$.

For minimum bias simulation, the background has to be fitted with a quadratic function :

$$b\left(E\right) = \frac{1}{N_{norm,b}} \cdot \frac{N_b}{N_{bin}} \cdot \left[1 + a_b\left(E - E_0\right) - b_b\left(2\left(E - E_0\right)^2 - 1\right)\right] \tag{11}$$

with

$$N_{norm,b} = N_b\left(b_b + 1 - \frac{b_b}{6}(\Delta E)^2\right) \tag{12}$$

with $\Delta E = E_{max} - E_{min}$, and the parameters of the fit are now :

P_0	$\rightarrow$	N_s	:	Number of signal counts
P_1	$\rightarrow$	M	:	Mass of the K^{0*}
P_2	$\rightarrow$	Γ	:	Width of the K^{0*}
P_3	$\rightarrow$	N_b	:	Number of background counts
P_4	$\rightarrow$	a_b	:	Background slope
P_5	$\rightarrow$	b_b	:	Background quadratic parameter

The fit is shown on Figure 11 and its parameters in Table 2. The background is much more difficult to subtract in this new case, since we have K^{0*} candidates coming from all possible $K^+\pi^-$ combinations. Because we couldn't access to the "MC-truth" information like in the first case, the cuts were decided with the help of the informations on the quality of the fit (χ^2, ratio signal over error, efficiency) (Table 2). The values of the parameters are compatible with the PDG informations (Table 1), but we must not forget that this is simulation data, and these parameters have been explicitly put as initial parameters.

6 Real LHCb data

Finally we applied the previous cuts on the real data, which were taken at LHCb in April 2010 ; the energy in the center of mass is 7 TeV and it contains 16.37 millions of events. No re-optimization of the cuts was necessary. The fit obtained is shown in Figure 13 and its parameters in Table 2. Surprisingly, we get better signal over noise ratio with real data than minimum bias Monte-Carlo (!). Several explanations can be given as hypotheses for this behaviour. First of all, the energy is not the same for real and simulation data (7 TeV for real data, 10 TeV for Monte-Carlo) ; we can imagine that at 10 TeV there is more background. Then, we have to be careful comparing the results, because we don't have the same number of entries for the two fits, and thus, not the same errors (the error following the square root of the number of entries). But the number of entries is not that different, so maybe this is not the main reason why we get better results than with simulation.
The parameters are still quite compatible with the PDG values.

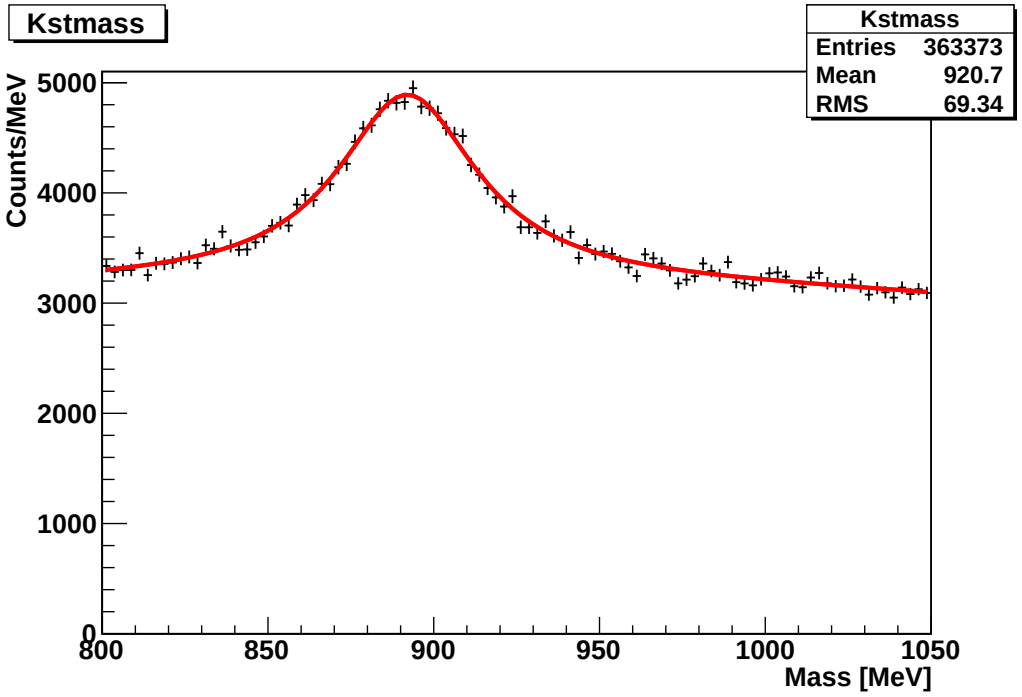

Figure 13: $K(892)^{0*}$ peak, real data

	Simulation data		Real data
	Preselected	Minimum bias	
Efficiency	19.37 %	1.04 %	0.29 %
χ^2	1.3	1.1	1.0
$P_0/\sigma(P_0)$	24.9	17.0	27.0
P_0	1898± 76	34404 ± 2029	47103 ± 1748
P_1	896.1 ± 0.8	895.2 ± 0.7	892.0 ± 0.4
P_2	47.4 ± 2.8	60.7 ± 2.8	51.3 ± 1.8
P_3	883 ± 70	391816 ± 2126	316269 ± 1819
P_4	$(29.0 \pm 4.9)10^{-4}$	$(-22.6 \pm 3.0)10^{-5}$	$(-15.1 \pm 3.5)10^{-5}$
P_5	-	$(7.3 \pm 2.8)10^{-7}$	$(7.1 \pm 3.1)10^{-7}$

Table 2: Parameters of the fit for the different data types

7 A few characteristics of K^{0*} in LHCb data

Now that we have our signal, we can observe its characteristics. If we assume that the background is linear and that the peak is mostly contained between 820 MeV and 960 MeV, we can deduce the signal characteristics the following way. We look at the 820-960 MeV range ; in it we have all the signal plus some background. Then we look at the 750-820 and 960-1030 MeV range where we assume we have as much background as we had in the 820-960 MeV, but with no signal. If we take the K^{0*} momentum for instance, we create a histogram for "signal + background" and a second one for the background. Then we create a new histogram with the difference between the first and the second, and in which we thus have only signal (roughly). The distributions for the momentum, transverse momentum and distance to the PV for the K^{0*} are given in Figures 14, 15 and 16.

The momentum distribution is peaked around 20 GeV, but we see that the mean momentum is higher for the signal than for the background : the high momenta are dominated by the signal. This effect is even more important for transverse momenta. But in the case of the distance to PV, it is peaked at 0 and the tail of distribution is dominated by the background. The longest distances to the PV, for the signal, belong to K^{0*} that are mostly coming from B or from D (i.e. which are not prompt).

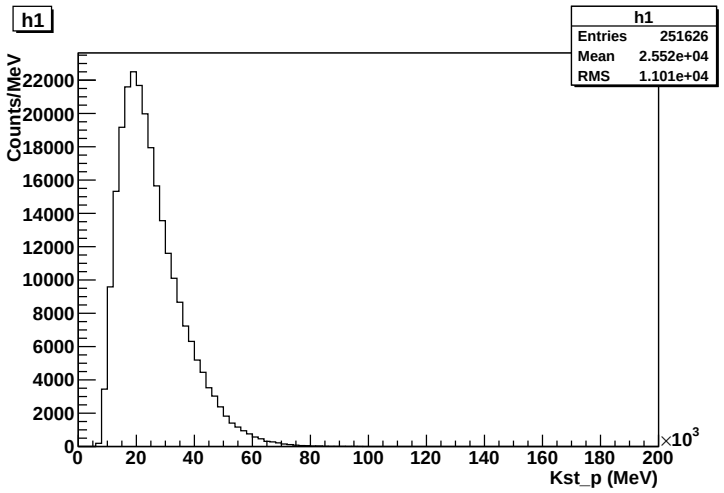

(a) Signal + background

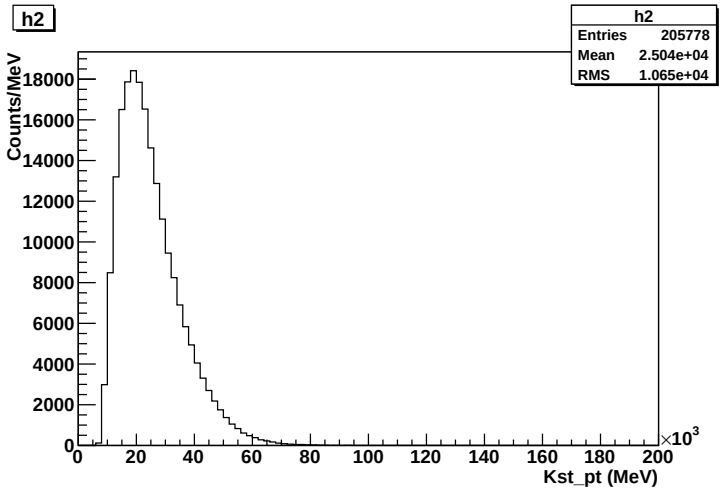

(b) Background

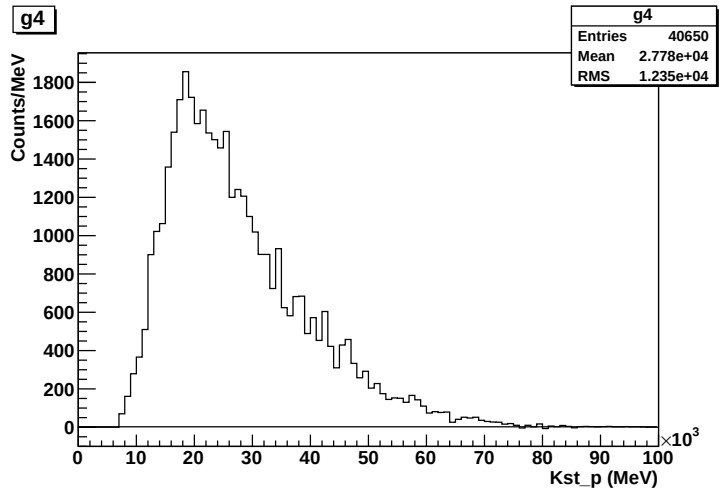

(c) Signal

Figure 14: K^{0*} momentum distribution

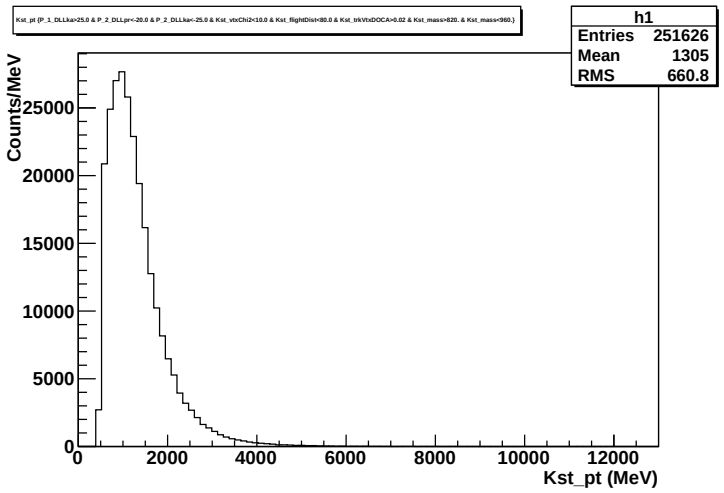

(a) Signal + background

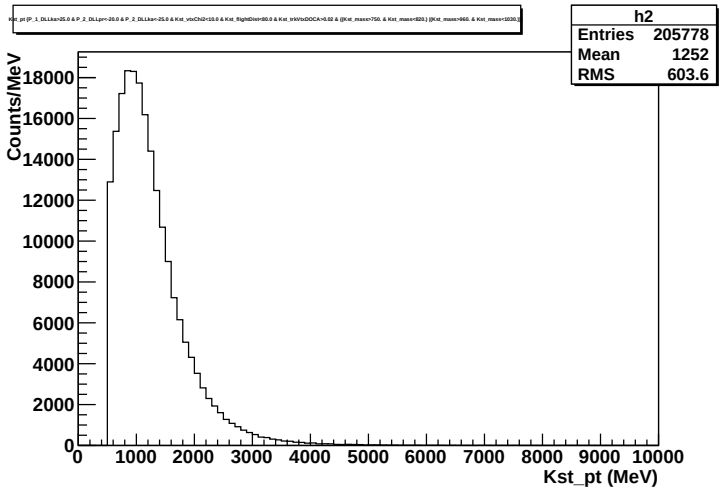

(b) Background

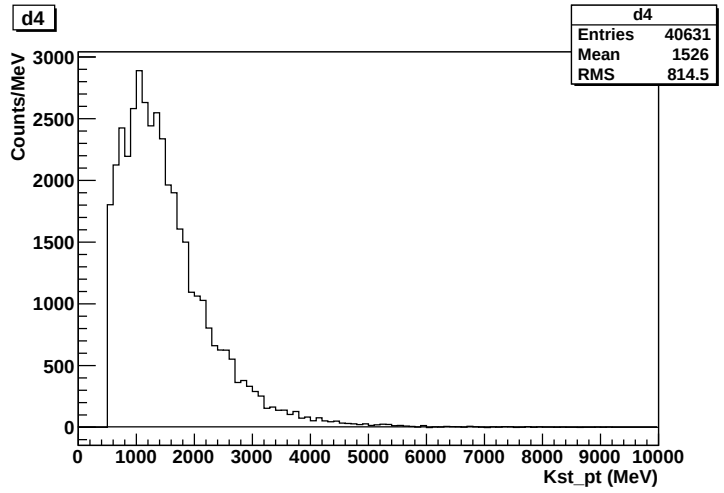

(c) Signal

Figure 15: K^{0*} transverse momentum distribution

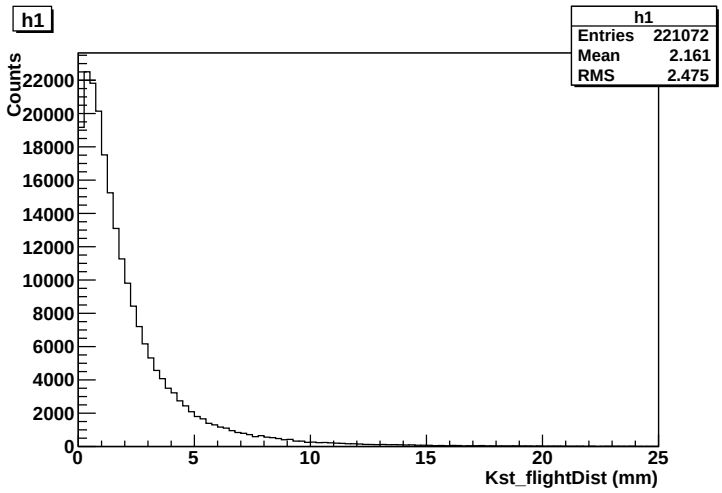

(a) Signal + background

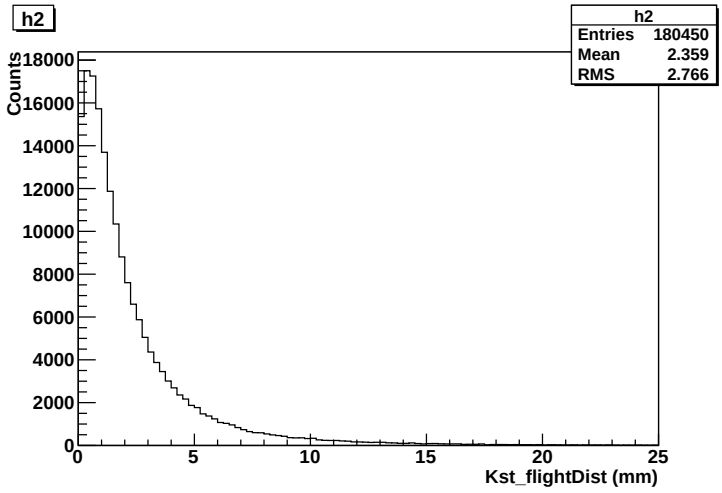

(b) Background

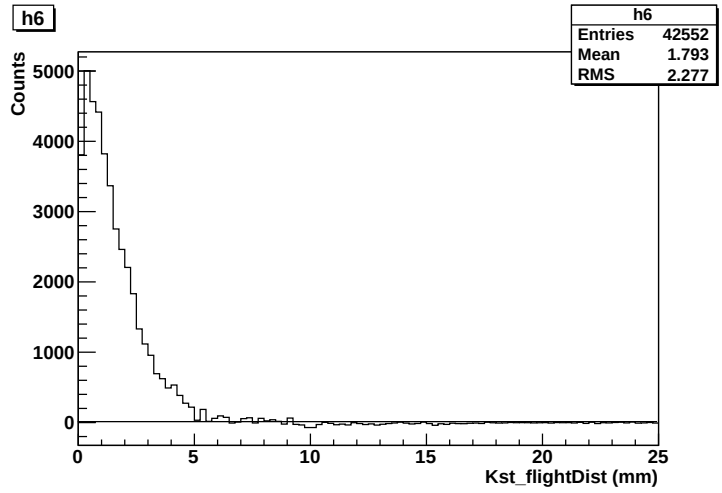

(c) Signal

Figure 16: K^{0*} distance to PV distribution

8 Conclusion

After this work, we are now able to see the inclusive $K(892)^{0*}$ signal from the first data taken at LHCb. To optimize the cuts, it would have been good to see the real distributions of the variables for the true K^* for minimum bias Monte-Carlo ; but even without it we have a relatively clean signal. We can now look at the characteristics of the K^{0*} in LHCb at 7 TeV. The informations about K^* momentum, transverse momentum and distance from the PV are given above as example.

References

[1] LHCb public website : http://lhcb-public.web.cern.ch/lhcb-public

[2] Particle Data Group, *Particle Physics Booklet*, July 2008 (http://pdg.lbl.gov/2009/tables/contents_tables.html for the 2009 updates)

[3] ROOT website : http://www.root.cern.ch

[4] Pr. Olivier Schneider, *Introduction à la Physique Nucléaire et Corpusculaire*, lecture notes